

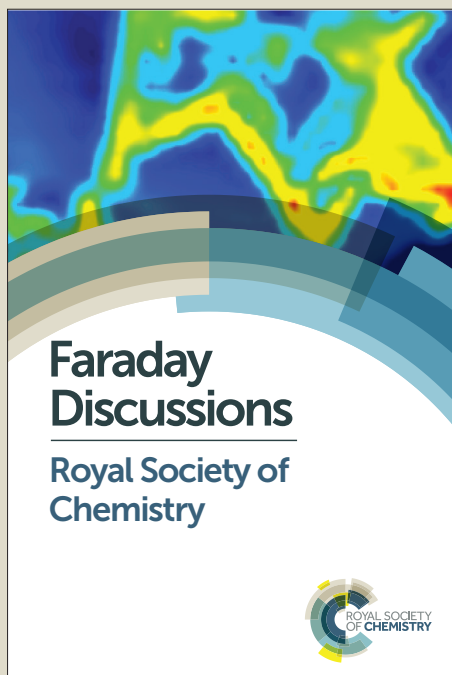
Faraday Discussions

Accepted Manuscript



This manuscript will be presented and discussed at a forthcoming Faraday Discussion meeting. All delegates can contribute to the discussion which will be included in the final volume.

Register now to attend! Full details of all upcoming meetings: <http://rsc.li/fd-upcoming-meetings>



This is an *Accepted Manuscript*, which has been through the Royal Society of Chemistry peer review process and has been accepted for publication.

Accepted Manuscripts are published online shortly after acceptance, before technical editing, formatting and proof reading. Using this free service, authors can make their results available to the community, in citable form, before we publish the edited article. We will replace this *Accepted Manuscript* with the edited and formatted *Advance Article* as soon as it is available.

You can find more information about *Accepted Manuscripts* in the [Information for Authors](#).

Please note that technical editing may introduce minor changes to the text and/or graphics, which may alter content. The journal's standard [Terms & Conditions](#) and the [Ethical guidelines](#) still apply. In no event shall the Royal Society of Chemistry be held responsible for any errors or omissions in this *Accepted Manuscript* or any consequences arising from the use of any information it contains.

Ruthenium Catalysts for Water Oxidation

Involving Tetradentate Polypyridine-type Ligands

Lianpeng Tong, Ruifa Zong, Rongwei Zhou, Nattawut Kaveevivitchai,

Gang Zhang and Randolph P. Thummel*

Department of Chemistry, 110 Fleming Building, University of Houston,

Houston, TX 77204-5003

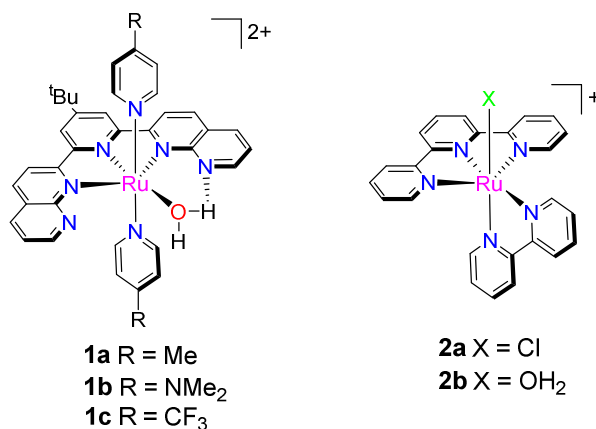
thummel@uh.edu

Abstract

A series of Ru^{II} complexes that behave as water oxidation catalysts were prepared involving a tetradentate equatorial ligand and two 4-substituted pyridines as the axial ligands. Two of these complexes were derived from 2,9-di-(pyrid-2'-yl)-1,10-phenanthroline (dpp) and examine the effect of incorporating electron-donating amino and bulky *t*-butyl groups on catalytic activity. A third complex replaced the two distal pyridines with N-methylimidazoles that are more electron-donating than the pyridines of dpp and potentially stabilize higher oxidation states of the metal. The tetradentate ligand 2-(pyrid-2'-yl)-6-(1'',10''-phenanthrol-2''-yl)pyridine (bpy-phen), possessing a bonding cavity similar to dpp, was also prepared. The Ru^{II} complex of this ligand does not have two rotatable pyridines in the equatorial plane and thus show different flexibility from the [Ru(dpp)] complexes. All the complexes showed activity towards water oxidation. Investigation of their catalytic behavior and electrochemical properties suggests that they may follow the same catalytic pathway as the prototype [Ru(dpp)pic₂]²⁺ involving a seven-coordinated [Ru^{IV}(O)] intermediate. The influence of coordination geometry on catalytic performance is analyzed and discussed.

Introduction

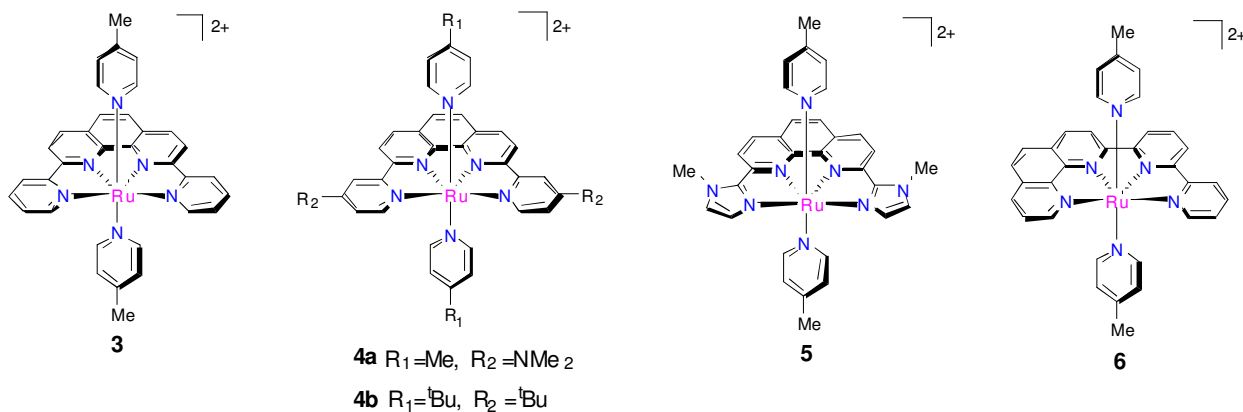
One of the more challenging goals in the area of artificial photosynthesis has been the design of a robust, efficient catalyst for water oxidation. Considerable recent activity in this area has been focused on metal-based systems and more recently on mononuclear coordination complexes involving metals such as Ru^{II}, Co^{III} and Ir^{III}.¹ With regard to mononuclear Ru^{II} polypyridine-type systems, several general types of catalyst have been reported. The first documented mono-nuclear Ru^{II} catalysts were complexes **1a-c** in which a water molecule occupying an equatorial site is stabilized by hydrogen bonding to an uncomplexed nitrogen of a peripheral 1,8-naphthyridine ring.² It was initially suspected that this H-bond might play an important role in activating the water molecule towards eventual oxidation. Modification of the axial pyridine appeared to exert a strong effect on the catalysis with electron donating substituents in the 4-position being more favorable.



A second class of mononuclear Ru^{II} catalyst was soon discovered based on the parent system [Ru(bpy)(tpy)Cl]⁺ (**2a**, bpy = 2,2'-bipyridine, tpy = 2,2'; 6',2''-terpyridine).³ Replacement of Cl⁻ by water was observed when **2a** was dissolved in aqueous solution. Thus the aqua Ru^{II} complex **2b** was proposed to be the authentic water oxidation catalyst.^{3d, e} For catalytic activity, it appeared that a tridentate ligand such as tpy was required, and variations on the bidentate

ligand indicated that electron-withdrawing substituents on bpy were preferable.^{3e} The structure-activity relationship for these types of complexes was supported by a proposed mechanism for the oxidation process which involves water attack on $[\text{Ru}^{\text{V}}=\text{O}]$ as the O–O bond formation step and O_2 release from $[\text{Ru}^{\text{IV}}-\text{OO}]$ as the rate-determining step.^{3f} The exact role of the halogen monodentate ligand in these systems is also the subject of some discussion.⁴

Following our initial report in 2008, we described a third class of mononuclear Ru^{II} catalyst involving a tetradentate equatorial dpp-type ligand (dpp = 2,9-di-(pyrid-2'-yl)-1,10-phenanthroline) complimented by two monodentate axial pyridines.⁵ An interesting feature of these tetradentate complexes was that they were *all* active as water oxidation catalysts with turnover numbers (TONs) in the range of 146-416 (after 48 h reaction). In examining a series of dinuclear Ru^{II} water oxidation catalysts, we had noticed that with N-methylimidazole as the axial dative ligand, the complexes showed no water oxidation activity.⁶ Contrarily, when N-methylimidazole was appended to the 2,9-positions of 1,10-phenanthroline (phen) to provide the complex **5**, the catalyst showed good activity (TON = 281). In our previous work, however, the structure-activity relationship of mononuclear complexes such as **3**, **4a** and **5** was not elucidated due to insufficient understanding of the catalytic mechanism.



Ruthenium Catalysts for Water Oxidation Involving Tetradentate Polypyridines

Recently, Sun and coworkers have reported two closely related mononuclear water oxidation catalysts having tetradentate equatorial ligands: a 6,6'-dicarboxy-bpy and a 2,9-dicarboxy-phen.⁷ In either case, the ruthenium complex associated with water when oxidized to Ru^{III} or Ru^{IV} state, and the [Ru^{IV}-OH]⁺ species was observed as an intermediate in the catalytic cycle. It was also discovered that rather subtle differences in the flexibility of the ligand structure led to a dramatic change in mechanism with the bpy-based system functioning through a bimolecular O-O coupling pathway while the more rigid phen-based system undergoes nucleophilic attack of water on a [Ru^V=O] species. The diverse pathways were ascribed to the difference in rigidity between 6,6'-dicarboxy-bpy and 2,9-dicarboxy-phen ligands.^{7b}

More recently, catalytic water oxidation by **3** was extensively examined using a combination of experimental and theoretical methods.⁸ It was suggested that, after oxidation to the Ru^{IV} state, the complex is able to access a seven-coordinated 18e [Ru^{IV}(O)]²⁺ via water association and a two proton coupled one electron transfer step. The formal Ru^{IV}=O intermediate subsequently initiates the catalytic cycle. Similar to the closely related systems reported by Sun and coworkers, it should be noted in the two x-ray structures earlier reported for **3** and **5** that the N-Ru-N angle exterior to the three fused chelate rings is considerably larger (*ca.* 125°) than the 90° expected for an unstrained tetradentate equatorial geometry.⁵ This feature in the structures of **3** and **5** allows a water molecule to enter the coordination sphere in the equatorial plane by bisecting the exocyclic N-Ru-N angle. It appears that all six ligating Ru-N bonds in the tetradentate complexes under study are fairly stable in water and do not show any propensity of water/N(pyridyl) exchange. This stability is verified by their proton NMR in water and recovery of the UV-vis absorption in a titration experiment.⁸

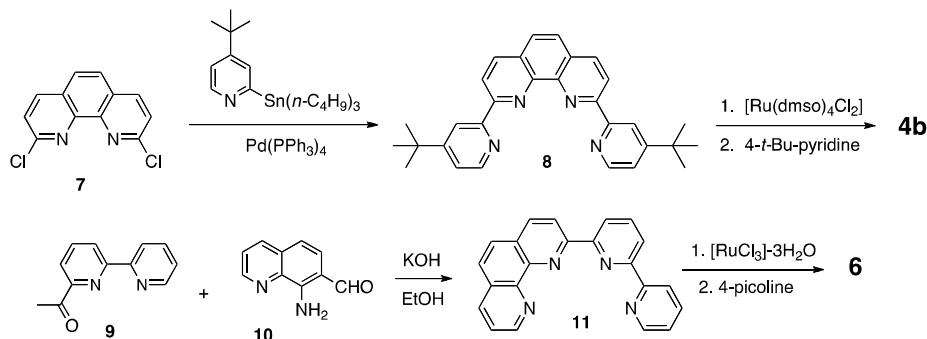
In this paper we will elaborate on some of the systems presented in our earlier work, **3**, **4a** and **5**, as well as the related tetradentate catalysts **4b** and **6** that were designed to help elucidate mechanism and optimize performance. We have noticed that when 4,4',4''-tri-*t*-butyl-tpy is substituted for tpy in catalyst **2a**, the catalytic activity in the cerium ammonium nitrate (CAN)-driven O₂-evolution significantly improves,^{4a} suggesting that the bulky, non-oxidizable *t*-butyl groups may inhibit decomposition of the catalyst. In this regard, two *t*-butyl groups were introduced on the equatorial ligand of **4b**. From our earlier work with catalysts **1a-c** we had learned that better activity was provided by systems having an electron-donating substituent at the pyridine 4-position. This is probably because the electron donors facilitate electron transfer steps in the catalytic cycle. The effect of Me₂N- group in **4a**, which is supposed to be a stronger electron donor than the methyl or *t*-butyl groups, will be examined in terms of its catalytic rate. N-methylimidazole in **5** is a better electron donor than pyridine in complex **3**.^{1h, 9, 10} Finally we have prepared a 2-(pyrid-2'-yl)-6-(1'',10''-phenanthroline-2''-yl)pyridine (bpy-phen, **11**) and its corresponding Ru^{II} complex **6** to further probe the role of steric strain in modulating the activity of water oxidation catalysts.

Synthesis and Characterization

The preparation and characterization of complexes **3**, **4a** and **5** have been reported previously.^{5, 11} The ligand 2,9-di(4'-*t*-butylpyrid-2'-yl)phen (**8**) was prepared by the Stille coupling of 4-*t*-butylpyrid-2-yl)-tri-*n*-butyl stannane with 2,9-dichlorophen (**7**). This material was readily characterized by the downfield region of its ¹H NMR that showed six equal area peaks: two doublets for H5' and H6' (*J* = 5 Hz), two doublets for H3 and H4 (*J* = 8.5 Hz), and two singlets for H3' and H5. Subsequent treatment of **8** with RuCl₃ followed by the addition of

excess 4-*t*-butylpyridine afforded the complex **4b**. This complex showed a pair of doublets at higher field each integrating for the 4 aromatic protons of the two axial pyridines. The 12 protons on the equatorial ligand were all well resolved with H6' appearing at 10.15 ppm (Figure S1).

Scheme 1. Synthesis of **4b** and **6**.



The ligand 2-(pyridin-2-yl)-6-(1,10-phenanthroline-2-yl)pyridine (**11**) was prepared in 97% yield through the Friedländer condensation of 2-acetylpyridine (**9**) with 8-amino-7-quinolinecarbaldehyde (**10**). This material was readily identified by its well resolved ^1H NMR spectrum which clearly showed all 14 protons as part of 5 independent spin systems. The ligand was then treated first with RuCl_3 to incorporate the metal and subsequently with 4-picoline to install the two axial picolines. This resulting complex **6** was characterized by its ^1H NMR (Figure S2) as well as its X-ray crystal structure (Figure 1).

The proton NMR spectrum of $\mathbf{3}(\text{Cl}^-)_2$ in D_2O shows seven peaks for the 14 aromatic protons of dpp ligand, consistent with C_{2v} symmetry. The addition of acetonitrile (5%, v/v), however, breaks the symmetry due to the association of acetonitrile molecule to the Ru center and dissociation of one pyridyl sub-unit of the equatorial ligand (Figure S3). In contrast, the acetonitrile/pyridyl ligand exchange does not occur for complex $\mathbf{6}(\text{Cl}^-)_2$. Its proton NMR

Ruthenium Catalysts for Water Oxidation Involving Tetradentate Polypyridines

spectrum in D₂O is unchanged in the presence of acetonitrile (Figure S2). The different behavior of these two complexes towards acetonitrile association is intriguing, considering the very similar sizes of the tetradentate ligands dpp and bpy-phen (**11**). Both distal pyridyl moieties of dpp might contribute to the association of acetonitrile by torsion about the 2,2'-bond. By comparison, the rigid phen moiety of the bpy-phen in complex **6** prohibits some of this torsional strain. To avoid the interference from acetonitrile coordination, it was not employed as a co-solvent in the study of O₂ evolution catalysis.

Table S1 summarizes the electronic absorption properties of the tetradentate Ru complexes presented in this work and Figure S4 illustrates the absorption spectra in water of the complexes **4b**(Cl⁻)₂ and **6**(Cl⁻)₂. The strong absorbance at 450-600 nm for these complexes is assigned to a metal-to-ligand transition involving charge transfer to the more electronegative tetradentate equatorial ligand. Although the bpy-phen ligand in complex **6** contains a C11-C16 single bond between the bpy and phen sub-units, chelating with Ru^{II} keeps the ligand planar and allows for efficient charge delocalization over both bpy and phen moieties. As a result, the 564 nm absorption of **6** closely resembles a Ru(dpp)-type complex. It should be noted that due to solubility issues the absorbance of complexes with PF₆⁻ counter ions were measured in acetone while those with Cl⁻ counter ions were measured in water. The medium has some influence on the electronic absorption of these complexes. The absorption profiles of **6** in pH = 1.0 HNO₃ and pH = 10.5 phosphate buffer (Figure S5) do not show distinctive difference, ruling out the replacement of a nitrogen donor of **6** by water and the formation of an aqua species which usually displays different absorption spectra under acidic and basic conditions caused by proton association or dissociation.

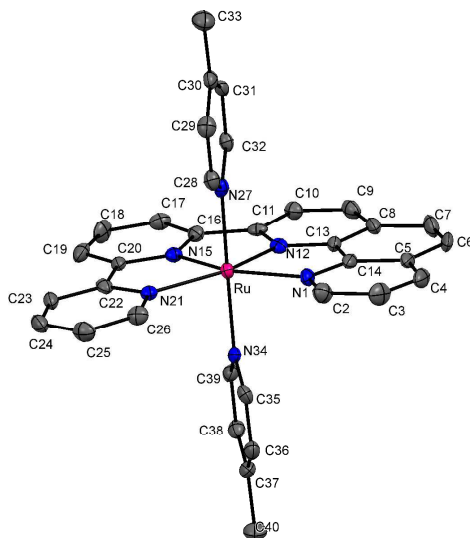


Figure 1. Thermal ellipsoid plot representation of crystal structure of $\mathbf{6}(\text{Cl})_2$ at 50% probability; non-polar hydrogen atoms, fractional solvent and Cl^- counter ion are omitted for clarity; color code: ruthenium (magenta), nitrogen (blue), and carbon (grey).

Table 1. Selected bond distances (\AA), bond angles ($^\circ$) and dihedral angles ($^\circ$) for the solid structure of $\mathbf{6}(\text{Cl})_2$.

Bond distance (\AA)	
Ru–N1	2.178(4)
Ru–N12	1.946(4)
Ru–N15	1.960(4)
Ru–N21	2.145(4)
Ru–N27	2.099(4)
Ru–N34	2.094(3)
Bond angles ($^\circ$)	
N1–Ru–N21	122.3(2)
N1–Ru–N12	79.3(2)
N12–Ru–N15	79.8(2)
N15–Ru–N21	78.5(2)
N27–Ru–N34	174.4(2)
Dihedral angles ($^\circ$)	
N21–C22–C20–N15	1.70
N15–C16–C11–N12	1.20
N12–C13–C14–N1	0.42

The solid state structures of **3** or **5** have been published previously.⁵ Figure 1 depicts the structure of complex **6**(Cl)₂. All three complexes adopt a distorted octahedral geometry. The four Ru-N bonds in the equatorial plane appear as two short bonds and two long ones. The internal Ru-N bonds to N12 and N15 are shorter (1.946 and 1.960 Å) while the external bonds to N1 and N21 are longer (2.178 and 2.145 Å). The Ru-N bonds to the axial picolines are intermediate at 2.094 and 2.099 Å. The N-Ru-N angles in the equatorial plane show considerable variation. The three internal angles fall in the range of 78.5-79.8°, all considerably less than the optimal octahedral angle of 90°. The external N-Ru-N angle is unusually large at 122.3°, providing an avenue for attack by water in the equatorial plane. The phen-bpy ligand is relatively planar in the complex. If one considers the dihedral angles associated with the three internal five-membered chelate rings, these range from 1.70° for the bpy containing chelate ring to 0.42° for the phen contained chelate ring. The central five-membered chelate ring is intermediate at 1.20°. The approximate planarity of the phen-bpy ring is further supported by the summation of the four N-Ru-N angles in the equatorial plane which is 359.9°. The two picolines are arranged in a slightly non-linear fashion with the N27-Ru-N34 angle being 174.4°. These features are all quite similar to what was observed for the structures of **3** and **5**.⁵

Electrochemical Study

Cyclic voltammograms (CVs) of **3**, **4a** and **5** in acetonitrile were reported earlier (Table 2), and showed reversible redox waves corresponding to the Ru^{II}/Ru^{III} process. Due to the electron-donating effect of the dimethylamino substituent, the $E_{1/2}^{\text{ox}}$ of **4a** (1.18 V vs SHE, all potential values in this paper are referred to SHE) is substantially lower than that of **3** (1.48 V) or **5** (1.30 V). CVs of **4b** and **6** in acetonitrile were measured in this work (Figure S6). Their

$\text{Ru}^{\text{II}}/\text{Ru}^{\text{III}}$ redox potentials, 1.49 V and 1.43 V respectively, are quite close to that of **3**. Apparently, extra *t*-butyl groups in the ligands of **4b** do not exert significant, if any, electronic effect upon the complex as compared to complex **3**.

Table 2. Redox potential for Ru^{II} complexes in organic and aqueous medium.

Complexes	$E_{1/2}^{\text{ox}}$ (V vs SHE) ^a in acetonitrile	E^{ox} (V vs SHE) at pH = 1.0
3 (PF ₆ ⁻) ₂ /(OTf ⁻) ₂	1.48 ^b	1.08 ^d , 1.25 ^d
4a (PF ₆ ⁻) ₂	1.18 ^b	0.90 ^e , 1.19 ^e
4b (PF ₆ ⁻) ₂	1.49 ^c	1.00 ^e , 1.19 ^e
5 (PF ₆ ⁻) ₂	1.30 ^b	0.84 ^e , 1.06 ^e , 1.28 ^e
6 (ClO ₄ ⁻) ₂	1.43 ^c	1.01 ^e , 1.21 ^e

^aMeasured by cyclic voltammetry, $E_{1/2} = (E_{\text{pa}} + E_{\text{pc}})/2$. ^bCited from reference 5b, using SCE = 0.24 V vs SHE for conversion of the reference electrode. ^cThis work, using ferrocene ($E^{+1/0} = 0.69$ V vs SHE) as external reference. ^dCited from reference 8. ^eThis work; measured by square wave voltammetry in HNO₃ (containing 20% CF₃CH₂OH, overall pH = 1.0); using [Ru(bpy)₃]Cl₂ ($E^{+1/0} = 1.26$ V vs SHE) as external reference.

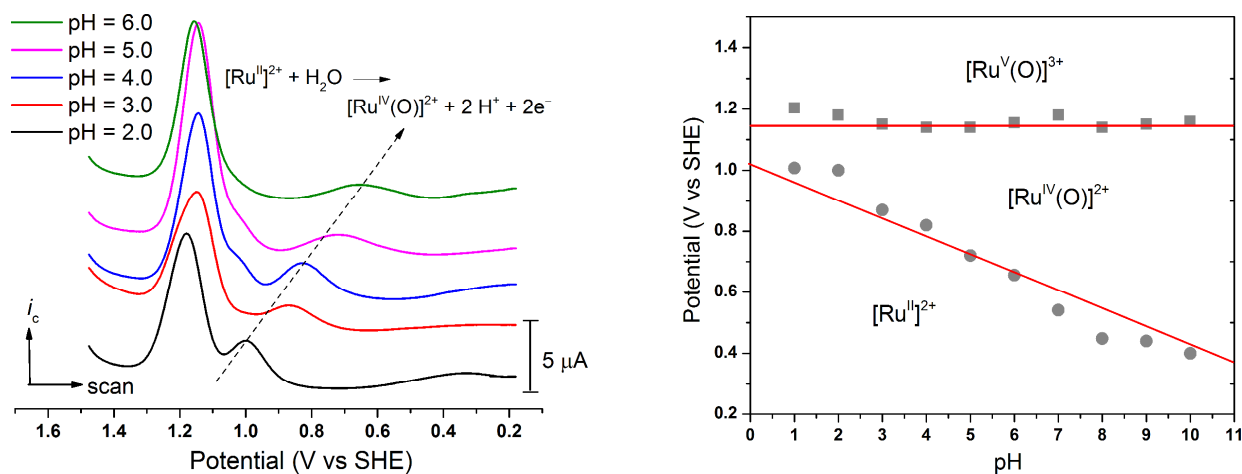
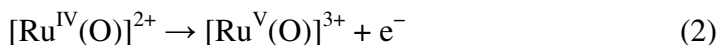
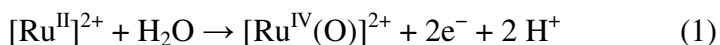


Figure 2. Left: Square wave voltammograms of **6**(ClO₄⁻)₂ recorded in the pH range 2-6. Right:

Pourbaix diagram of **6**(ClO₄⁻)₂.

The redox properties of complex **3** in aqueous medium have been investigated by combined experimental and theoretical methods and reported previously.⁸ While **3** undergoes a redox sequence of $[\text{Ru}^{\text{II}}]^{2+} \rightarrow [\text{Ru}^{\text{III}}]^{3+} \rightarrow [\text{Ru}^{\text{V}}(\text{O})]^{3+}$ under acidic conditions ($\text{pH} < 3$), a redox sequence of $[\text{Ru}^{\text{II}}]^{2+} \rightarrow [\text{Ru}^{\text{IV}}(\text{O})]^{2+} \rightarrow [\text{Ru}^{\text{V}}(\text{O})]^{3+}$ is instead favored at $\text{pH} > 3$. The redox behavior of **3** related to the pH of surroundings is the consequence of changes of thermodynamics for certain proton coupled electron transfer (PCET) steps depending on pH. In this study, redox properties of complex **6** were examined using CV and square wave voltammogram (SW) in aqueous solutions over the pH range from 1 to 10. As displayed in Figure 2, two consecutive redox events were revealed in the square wave voltammograms that were scanned from anode to cathode. While the potential of the first event at about 1.21 V vs SHE is independent of pH, the potential of the subsequent event is linearly dependent on pH with a slope of -59 mV/pH over the range of $\text{pH} = 1-10$. From this finding it is suggested that complex **6** follows a $[\text{Ru}^{\text{II}}]^{2+} \rightarrow [\text{Ru}^{\text{IV}}(\text{O})]^{2+} \rightarrow [\text{Ru}^{\text{V}}(\text{O})]^{3+}$ oxidation sequence in $\text{pH} = 1-10$ aqueous solutions, involving a $2\text{H}^+/2\text{e}^-$ PCET (Eq. 1) and a 1e^- ET (Eq. 2) steps.



SWs of **4a** and **4b** also show two redox waves at around 1.00 V and 1.20 V (Table 2 and Figure S7). The SW of **5**, however, exhibits another redox wave at 0.84 V besides the redox waves at 1.06 V and 1.28 V. Considering the similar ligand environment among complexes **3-6**

and referring to the electrochemical study upon **3** and **6**, we assign the redox event of **4a**, **4b** and **5** at about 1.00 V as formation of Ru^{IV} species and the redox event at about 1.20 V as formation of Ru^V species. In addition, the redox event of **5** at 0.84 V might correspond to a Ru^{II}/Ru^{III} process. We conclude tentatively that all complexes **3-6** could be oxidized to Ru^V state in pH = 1.0 aqueous solution given an applied potential more positive than 1.20 V; the intermediates involved in the Ru^{II} to Ru^V oxidation process may vary from one complex to another.

Water Oxidation

Ru^{II} complexes can be evaluated for their ability to catalyze the oxidation of water by exposing them to a large excess (≥ 1000 equivalents) of ceric ammonium nitrate (CAN) at low pH and monitoring the evolution of oxygen by a variety of techniques. In this work, a pressure transducer in the headspace of the reaction vessel was employed to monitor the real-time O₂ generation, while gas chromatography is used to analyze and verify the overall amount of O₂ evolved at the end-point of each run. Using these techniques, we have studied the kinetics of O₂ evolution by catalysts **3-6** and the results are summarized in Figure 3 and Table 3.

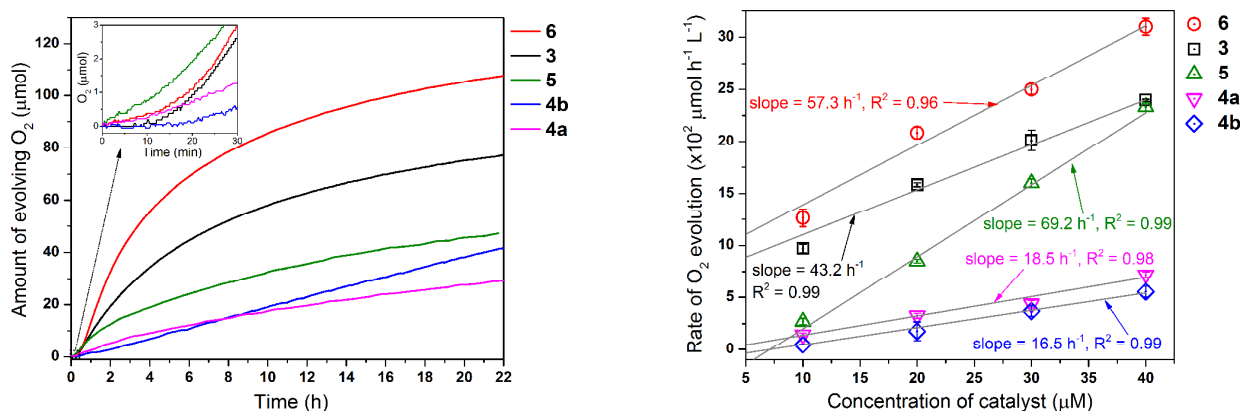


Figure 3. Left: O₂ evolution vs time plots (inset is enlarged 0 to 30 min). Conditions: 20 μM catalyst and 0.2 M CAN in 10 mL HNO₃ (pH 1.0). Right: Initial rate of O₂ evolution vs concentration of the catalyst (10~40 μM). The initial rate was measured by fitting the O₂

evolution vs time plots as a linear line in the time period from 20 to 50 min (for **3**, **4a**, **5** and **6**) or 2 to 3 h (for **4b**).

Table 3. Kinetic data for CAN-promoted water oxidation by Ru^{II} complexes.

Complexes	3	4a	4b	5	6
$k_{\text{obs}} / \text{initial TOF (h}^{-1}\text{)}$	43.	18.	16.	69.	57.
$t^1)^a$	2	5	5	2	3

^aThe k_{obs} or initial TOF is derived from the slopes illustrated in Figure 3.

As illustrated in Figure 3, all the complexes **3-6** were able to catalyze O₂ evolution after they were introduced into the CAN solution (in pH = 1.0 nitric acid). Although O₂ evolution by these catalysts did not cease after the 22 h time window, the rate of O₂ evolution diminished during the reaction as indicated by the decrease of the slope of the O₂ evolution versus time plots (Figure 3). Complex **4b** with bulky *t*-butyl substituents, however, is an exception. The O₂ evolving plot of **4b** as a function of time is almost linear and shows little loss of catalytic activity over 22 hours of reaction, indicating the extraordinary stability of **4b** compared to other ruthenium catalysts in the series. Another notable phenomenon from the O₂ evolving experiments is that these complexes exhibit considerable induction periods which vary from about one or two minutes for complexes **4a** and **6** to about ten minutes for **3** and more than twenty minutes for **4b**. Only in the case of **5**, was instant O₂ evolution detected as soon as the catalyst was injected into the CAN solution and no induction time was observed. These induction periods are primarily attributed to the slow rate of initial oxidation of the catalysts to their [Ru^{IV}(O)] states which actually initiate the catalytic cycle. In our earlier study of complex **3** we were able to show that after the initiation period, the addition of additional portions of CAN resulted in an immediate increase in

O₂ evolution. The role played by the equatorial tetradentate ligand in the duration of this induction period is not yet clear.

The initial rates of O₂ evolution were measured at various concentrations (10–40 μM) for each catalyst (Figure S8-12). The value of initial rate was simulated by linearly fitting a segment (30–60 min after the induction time period) of the O₂ evolution versus time plot, assuming that consumption of either CAN or catalyst is negligible during the induction period. The initial rates of **3-6** showed linear dependence on their concentration (Figure 3) following a pseudo first-order kinetics expression for the reaction rate = $k_{\text{obs}} \times [\text{cat.}]$, where k_{obs} is the pseudo first order rate constant and [cat.] is concentration of the catalyst. Because the CAN is present in large excess (5,000 to 20,000 equiv), the concentration of CAN can be regarded as constant during the time when the O₂ evolution rate is simulated. Thus the initial turnover frequency (TOF) of complexes **3-6** can be estimated in terms of initial O₂-evolving rates as $\text{TOF} = k_{\text{obs}} = \text{rate}/[\text{cat.}]$ (Table 3). While all the complexes **3-6** show moderate catalytic activity with initial TOF/ k_{obs} of 16-70 per hour, the most active catalyst **5** ($k_{\text{obs}} = 69.2$) is about four times faster than the least active catalyst **4b** ($k_{\text{obs}} = 16.5$). There does not appear to be any correlation between the stability of a catalyst and its rate of reaction, since the longest lived catalyst **4b** gives the lowest initial TOF.

Light-driven Water Oxidation

We also tested the catalytic activities of these complexes for photochemical water oxidation in aqueous media. O₂ evolution was initiated by irradiating a mixture of catalyst, sensitizer [Ru(bpy)₃]Cl₂, and sacrificial electron acceptor Na₂S₂O₈ in Na₂SiF₆/NaHCO₃ buffer (pH 6.8, 0.01 M Na₂SiF₆) with blue LEDs (470 nm).¹⁴ The amount of O₂ was monitored by a Clark-type YSI electrode in real time and the total amount of O₂ evolved was quantified by GC.

Ruthenium Catalysts for Water Oxidation Involving Tetradentate Polypyridines

As shown in Figure 4, all four complexes showed catalytic activity in such a three-component system with **6** being the most active (9 ± 1 turnovers in 10 min) and **4a** and **4b** being the least active (5 ± 1 turnovers in 10 min). The electron is believed to transfer from excited sensitizer to persulfate and then from catalyst to the quenched sensitizer.¹⁵ Due to the emerging concern of *in situ* generation of nano-size particles which may play the role of an authentic catalyst, potential formation of RuO₂ under the conditions of photocatalysis was inspected by dynamic light scattering (DLS). No nanoparticles were detected (Figure S13) after the photocatalytic system was irradiated for 10 min, confirming the homogeneous catalysis of O₂ evolution by a molecular catalyst.

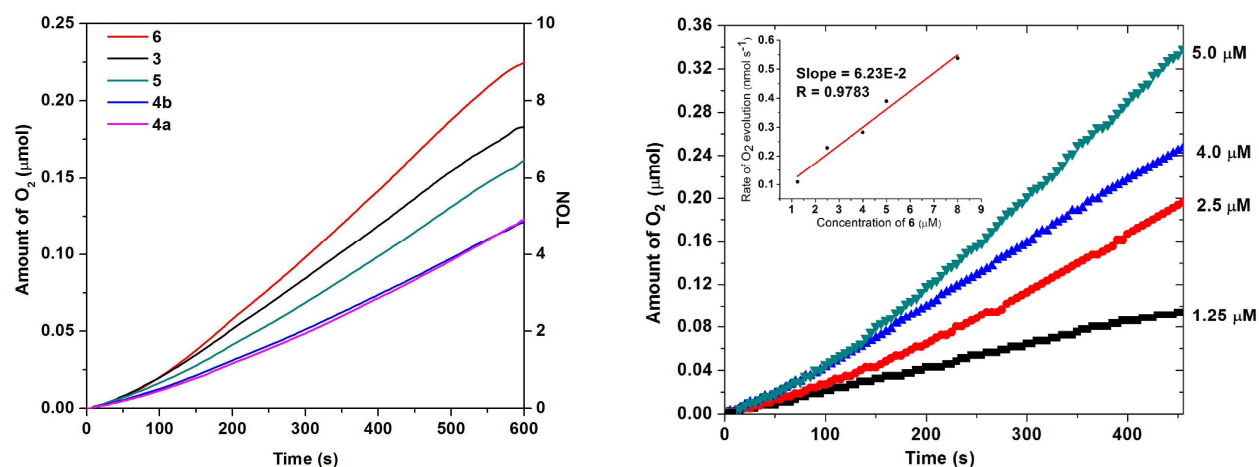


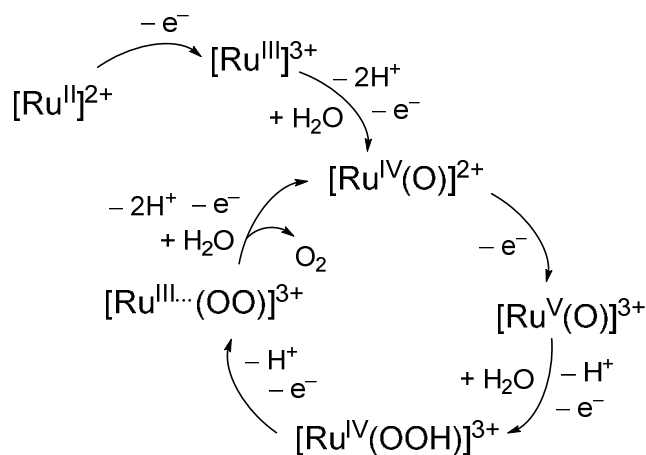
Figure 4. Left: Plots of O₂ evolution vs time in the photocatalytic water oxidation system containing [Ru(bpy)₃]Cl₂ (0.3 mM), Na₂S₂O₈ (10 mM) and catalyst **3-6** (2.5 μM) in pH = 6.8 Na₂SiF₆/NaHCO₃ buffer (5 mL, 0.01 M Na₂SiF₆) irradiated with blue LEDs (470 nm). Right: Initial rate of light-driven water oxygen at various concentrations of **6** (1.25 μM–8 μM), insert: the plot of initial rate of O₂ evolution vs concentration of **6**.

Initial rate of light-driven O₂ evolution varies linearly according to the concentration of **6** (1.25–8 μM) when the concentration of [Ru(bpy)₃]Cl₂ and Na₂S₂O₈ were held constant (Figure 4). The pseudo first-order kinetics of O₂ evolution for **6** are similar to what was observed in the CAN-promoted water oxidation, suggesting a similar single site catalytic pathway.⁸ Light-driven O₂ evolution by **6** ceased after about 10 min (Figure S14). Sun and coworkers have attributed the termination of O₂ evolution to the decrease in pH caused by the accumulation of protons in the photocatalytic system.¹⁷ However, the pH of the photocatalytic system in our work remained almost unchanged (pH 6.7) after 10 minutes of reaction. Moreover, the introduction of another portion of [Ru(bpy)₃]Cl₂ and Na₂S₂O₈ completely restarted light-driven O₂ evolution (Figure S14), indicating decomposition of the sensitizer as the major reason for the cessation of O₂ evolution under these conditions.¹⁸

Catalytic Pathway and Discussion

In an earlier report, we suggested that it might not be necessary to exchange water for one of the pyridyl donors of complex **3** in the initial period of catalytic water oxidation.^{3a} Rather, after oxidation of Ru^{II} to Ru^{IV} state, a water molecule might attack the electron deficient metal center in the equatorial plane of the tetradentate ligand to expand the coordination sphere to seven, giving a [N₆Ru^{IV}-OH₂]⁴⁺ species. Similar seven-coordinate high-valent Ru species have been characterized previously.¹² Moreover, Sun and coworkers recently reported a seven-coordinate [Ru^{IV}-OH₂] species as an intermediate in catalytic O₂ evolution system.^{7a}

Scheme 2. Proposed catalytic cycle for water oxidation by catalyst **3** at pH = 1.⁸



Following our previously reported calculations that support a seven-coordinate intermediate,^{3a} we recently revisited this catalyst using both experimental and theoretical techniques to disclose additional details about the mechanism of water oxidation catalyzed by **3**.⁸ According to the catalytic cycle proposed in Scheme 2, **3** was oxidized from Ru^{II} through Ru^{III} to [Ru^{IV}(O)] and [Ru^V(O)]. Notably, optimized structures for both [Ru^{IV}(O)] and [Ru^V(O)] intermediates favor seven coordinate pentagonal bipyramide geometries with C_{2v} symmetry. Subsequent addition of one water to [Ru^V(O)] occurs in concert with a $1e^-/H^+$ PCET to yield the [Ru^{IV}(OOH)]³⁺ species (Equation 3). The thermodynamic demand for this step is quite high (1.96 V at pH 0) and thus is suggested to be the slowest kinetic steps, explaining the long induction periods observed in the CAN-promoted O₂ evolution experiments at pH 1.0. Further oxidation of [Ru^{IV}(OOH)]³⁺ leads to the formation of [Ru^{III}... (OO)]³⁺, at which stage dioxygen dissociates from the ruthenium center.

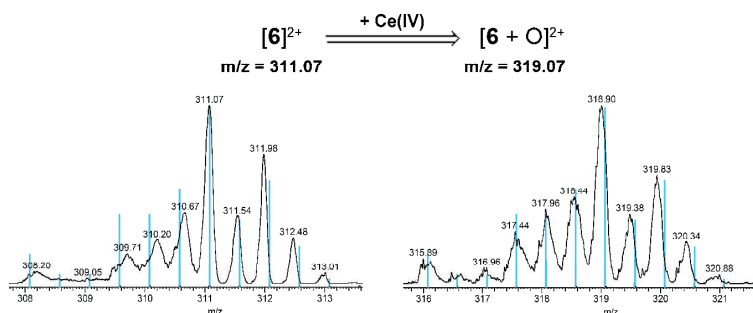


Figure 5. Observed and simulated (blue bars) mass spectra of ruthenium-containing species after treatment of **6**(Cl)₂ with 4 equivalents of CAN.

A key finding from the electrochemical study of **4a-6** is that they can be oxidized to $[\text{Ru}^{\text{V}}(\text{O})]^{3+}$ given the application of a positive enough potential. In the case of **6**, an oxidation sequence of $[\text{Ru}^{\text{II}}]^{2+} \rightarrow [\text{Ru}^{\text{IV}}(\text{O})]^{2+} \rightarrow [\text{Ru}^{\text{V}}(\text{O})]^{3+}$ was implied over the pH range 1-10 according to the Pourbaix diagram in Figure 2. The Ru^{III} species might be unstable respect to disproportionation over the broad pH range and thus ‘missing’ in the scenario.¹³ Furthermore, a ruthenium-containing species with a m/z value (318.90) corresponding to $[\mathbf{6}+\text{O}]^{2+}$ ($m/z = 319.07$) was evident in the mass spectrum, after treatment of **6** with 4 equivalents of CAN under acidic conditions (Figure S15, 16). It is assigned as the $[\text{Ru}^{\text{IV}}(\text{O})]^{2+}$ intermediate formed via the addition of one water molecule to **6** in concert with the loss of two protons and two electrons. The kinetics of O_2 evolution for **4a-6** resembles that of **3** as a pseudo-first order reaction suggesting a catalytic path via a single metal site. Taking into account the similar electrochemical and catalytic behaviors of **4a-6** and **3**, we propose that **4a-6** proceed through the same intermediates in their catalytic cycle as shown in Scheme 2.

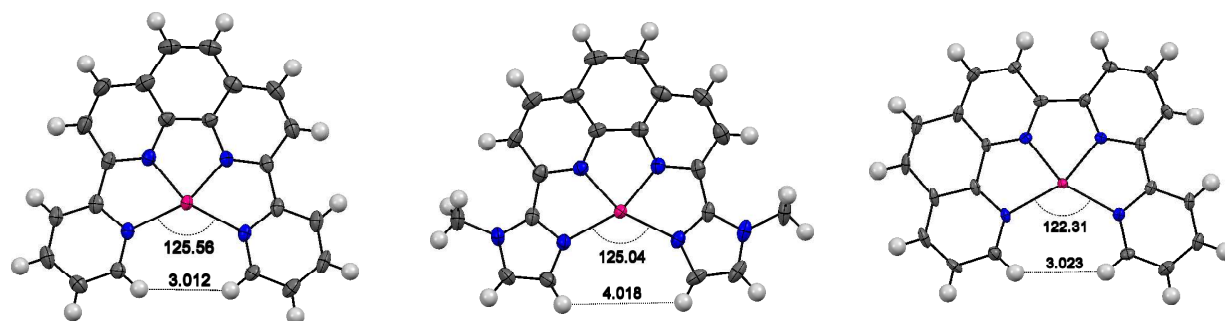


Figure 6. Thermal ellipsoid plot representation of planar fragment of **3** (left)^{5a}, **5** (middle)^{5b} and **6** (right, this work) at 50% probability; N-Ru-N angles ($^{\circ}$) and H-H distance (\AA) are marked; color code: ruthenium (magenta), nitrogen (blue), carbon (dark grey) and hydrogen (light grey).

Nevertheless, catalysts **3-6** demonstrate different reactivity towards water oxidation. The rate constant (k_{obs}) or initial TOF of **5** (69.2 h^{-1}) is significantly greater than the other systems. This increased reactivity is due to both steric and electronic factors associated with the equatorial ligands (Equation 3). On one hand, the larger N-Ru-N bite angle and the greater separation of the *ortho*-hydrogen atoms of **5** as compared to **3** or **6** (Figure 6) may cause less obstruction to water attack on the $[\text{Ru}^{\text{V}}(\text{O})]^{3+}$ species. On the other hand, the greater electron density of imidazole vs. pyridine may facilitate electron loss. Furthermore, the lack of any perceptible induction period in water oxidation catalyzed by **5** as compared to the other catalysts in the series is consistent with rate-limiting O-O bond formation (Eq. 3) being responsible for the induction period and the suggestion that **5** proceeds through this step faster than the others.

A much lower initial TOF of **4a** than that of **3** seems to imply a negative influence of the electron-donating amino group over the activity. It should be noted, however, that the difference of redox potentials between **4a** and **3** measured in pH 1.0 aqueous solution, if any, is substantially smaller than that in acetonitrile (Table 2). This is attributed to protonation of either or both of N,N-dimethyl amino groups in **4a** and therefore those amino substituents no longer

behave as electron donors. Enhanced stability of oxidation catalysts involving *t*-butyl groups has been noted in our earlier study.^{4a} It was for this reason that we prepared and examined the catalytic activity of **4b** which is a tetra-*t*-butyl analog of **3**. As shown in the water oxidation section (Figure 3), **4b** is more robust than **3** as well as other catalysts tested in the CAN-driven O₂ evolution experiments. After 22 h reaction, no salient loss of catalytic activity is observed for **4b**. The *t*-butyl groups can improve durability of catalyst in several ways. First, these *t*-butyl groups help to prevent ligand oxidation. Second, the hydrophobic property of *t*-butyl might suppress dissociation of the axial pyridyl ligand into the aqueous medium. Third, the bulky *t*-butyl group exerts a steric effect that makes the decomplexation of the distal pyridyl more difficult.

Conclusion

In conclusion, a series of mononuclear Ru^{II} complexes **4-6** has been synthesized and investigated as analogues of **3** which has been reported as a molecular water oxidation catalyst. Complexes **4-5** are proposed to catalyze water oxidation through a pathway similar to that of **3**. Some influence of coordination circumstance over the catalysis can be revealed by comparing the catalytic behavior of this group of complexes. Electron-donating ligands and great vacant space in the coordination sphere favor the catalytic activity by facilitating the highly energy-demanding water attack to [Ru^V=O] step. The *t*-butyl substituents depress the catalytic efficiency but enhance the stability of the catalyst. The phen-bpy ligand, compared with dpp, indicates that two rotatable distal pyridyl donors in the equatorial plane are not required regarding water oxidation. Findings in this work provide more evidence to our previous study about these WOCs

with tetradentate ligands and helps us to understand the relationship between their structure and activity.

Experimental Section

The ^1H NMR and ^{13}C spectra were recorded at room temperature on a JEOL ECX-400 or JEOL ECX-500s spectrometer at 400 MHz for ^1H and 100 MHz for ^{13}C . Chemical shifts are referenced to the residual solvent peak and were reported in parts per million (ppm) and the J values are ± 0.5 Hz. Melting points were measured on a Thomas Hoover capillary melting point apparatus and were not corrected. Electronic absorption spectra were recorded with a Varian Cary 50 Bio UV-visible spectrophotometer. All spectra were corrected for the background spectrum of the solvent. Mass spectra were obtained on a Thermo Finnigan LCQ DecaXP mass spectrometer using an ESI ionization source. Electrochemical measurements, including cyclic voltammetry and square wave voltammetry, were carried out under aerobic conditions and recorded with an BAS Epsilon potentiostation using a glassy carbon disk (diameter = 3 mm) as the working electrode, a platinum wire as the counter electrode, and a saturated calomel electrode (SCE) as the reference electrode. At pH = 1.0, a HNO_3 (with 20% $\text{CF}_3\text{CH}_2\text{OH}$ by volume) solution was employed as the electrolyte. Otherwise, the electrolytes were a series of phosphate buffers (0.1 M with 20% $\text{CF}_3\text{CH}_2\text{OH}$ by volume), of which the pH was adjusted by the addition of trifluoromethanesulfonic acid or NaOH solution. $[\text{Ru}(\text{bpy})_3]\text{Cl}_2$ ($E_{1/2} = 1.26$ V vs SHE) in aqueous medium) or ferrocene ($E^{+1/0} = 0.69$ V vs SHE) in organic medium was used as an external standard, and potentials were referenced to SHE. Dynamic light scattering (DLS) measurements were performed on a Zetasizer Nano ZS instrument (Malvern Instruments Ltd., U.S.A.) with a He-Ne gas laser (4 mW, λ 632.8 nm) light source, which can detect particles in

Ruthenium Catalysts for Water Oxidation Involving Tetradentate Polypyridines

the range from 0.6 to 6000 nm. Data were obtained using a scattering angle of 90 ° at 20 °C. A photocatalytic sample containing catalyst (2.5 μM), [Ru(bpy)₃]Cl₂ (0.3 mM), and Na₂S₂O₈ (10 mM) in the Na₂SiF₆/NaHCO₃ buffer (pH 6.8, 0.01 M Na₂SiF₆) was irradiated for 10 min before the DLS study. All reagents and solvents were purchased from commercial sources and were used as received except 2,9-dichloro-1,10-phenanthroline (**7**)¹⁹, 6-acetyl-2,2'-bipyridine (**9**)²⁰ and 8-amino-7-quinolinecarbaldehyde (**10**)²¹ that were prepared according to published procedures. The complexes **3**(Cl⁻)₂, **4a**(PF₆⁻)₂ and **5**(PF₆⁻)₂ have been described previously.⁵ CHN analyses were performed by Quantitative Technologies Inc., Whitehouse, NJ.

CAN-promoted water oxidation

CAN-promoted dioxygen evolution was performed using a custom-built 25 mL round bottom flask connected to a pressure transducer (Omega PXM409-002 BAUSBH, pressure range 0-2 bar) via a Teflon spacer. In a typical run, the custom-built flask was charged with 10 mL HNO₃ (pH = 1.0) containing [Ce(NO₃)₆](NH₄)₂ (1.09 g, 2 mmol) and a stirring bar. The flask was put into a water jacketed beaker, and the temperature was controlled to 20 °C by a temperature controller (VWR 1147P). The Ru(II) catalyst (100~400 μL, 1 mM) in water (for chloride complexes) or CF₃CH₂OH/water (v/v = 20/80, for PF₆⁻ complexes) was then introduced by syringe through a septum. During the course of a given run, the head space pressure was monitored in real-time using data acquisition software (TRH Central, Omega Engineering Inc) with a frequency of 5 s per reading. At the end of each reaction, a gas sample was taken from the head space of the flask and analyzed by gas chromatography (GOW-MAC Series 400 GC, , equipped with a 5X molecular sieve column and a TC detector, and operated with Ar as the carrier gas) to determine the amount of generated hydrogen. The initial rates were calculated by

Ruthenium Catalysts for Water Oxidation Involving Tetradentate Polypyridines

linear fitting of the plots of O₂ evolution (mmol) versus time (h) in certain time periods. The initial rate constants (h⁻¹) were estimated from the slope of the plot of the initial rate of oxygen evolution (mM·h⁻¹) versus the concentration of the catalyst (mM).

Light-driven water oxidation

All photocatalytic experiments were performed in a two-necked vessel (32 mL), with one neck anchored to a YSI 5331 Clark probe connected to a YSI- 5300A biological oxygen monitor and the other filled by a septum. A fresh teflon membrane over the YSI probe tip was exchanged after every 5 runs. The YSI probe was calibrated in oxygen-free water (N₂ purge, 0%), oxygen saturated water (O₂ purge, 100%) and air-saturated water (20 ± 1%). Stock solutions of [Ru(bpy)₃]Cl₂ (0.01 g in 2 mL, 7.8 mM), Na₂S₂O₈ (0.13 g in 1 mL, 0.55 M), and catalyst (in CH₃CN) were prepared. In a typical photolysis experiment, a small aliquot (100 uL) of [Ru(bpy)₃]Cl₂ solution, Na₂S₂O₈ solution, catalyst solution and 5 mL Na₂SiF₆/NaHCO₃ buffer solution (0.01 M, pH = 6.8) were added in the vessel so that the final concentration of [Ru(bpy)₃]Cl₂, Na₂S₂O₈ and catalyst were 0.3 mM, 10 mM, and 2.5 μM respectively. The vessel was placed in a water-jacketed beaker (20 °C) wrapped with a strip of 18 LED blue lights (λ_{max} = 470 nm). The 18 module LED light strip (blue or green) and a 12v DC power source were obtained from Creative Lighting Solutions (www.CreativeLightings.com - product code CL-FRS-1212IN-RGB). Each LED module consists of 3 light sources and the module was wired to allow the illumination of all 3 sources. The mixed solution was degassed by N₂ until the YSI reading reached 0%. The Na₂SiF₆/NaHCO₃ buffer solution is prepared by the addition of NaHCO₃ to the 0.01 M Na₂SiF₆ solution until its pH reached 6.8. The program “Bytewedge” (Fog Software, Inc., fogsoft.com) gave an O₂ reading every 5 s for up to 30 min. All TON, TOF

and rate values were calculated from as an average of three runs.

2,9-Di-(4'-*tert*-butylpyrid-2'-yl)-1,10-phenanthroline (8).

A solution of 2-(dimethylamino)ethanol (DMAE) (4.82 mL, 40 mmol) in hexane (125 mL) was cooled to 0 °C and treated dropwise with *n*-BuLi (2.5 M/hexane, 32.5 mL, 82 mmol). After the yellow mixture had been kept at 0 °C for 20 min, a solution of 4-*t*-butylpyridine (3 mL, 20.5 mmol) in hexane (25 mL) was added dropwise. After 2 h, the brown solution was cooled to -78 °C and treated with (*n*-Bu)₃SnCl (13.6 mL). The mixture was stirred for an additional one h at -78 °C then allowed to warm to room temp. After 16 h, the residue was cooled to 0 °C and water (75 mL) was added. The organic phase was extracted with CH₂Cl₂ and the combined organic phase was washed with water, dried over MgSO₄ and concentrated to afford a yellow oil (9 g, 74%). NMR analysis showed the presence of 4-*t*-butyl-2-tri-*n*-butylstannylpyridine (74%), along with 4,4'-di-*t*-butyl-2,2'-bipyridine (18%), and unreacted 4-*t*-butylpyridine (8%). Due to difficulties in separation, this mixture was used in the next step without further purification.

A mixture of 2,9-dichloro-1,10-phenanthroline (**7**, 660 mg, 3.5 mmol), the above described mixture (8.69 g), and [Pd(PPh₃)₄] (300 mg, 0.42 mmol) in toluene (12 mL) was refluxed under Ar for 48 h. The solvent was evaporated and a minimum amount of hexane (5 mL) was added. The insoluble material was removed by filtration and washed with hexane (5 mL). The hexane solution was concentrated and the resulting precipitate was collected by filtration, washed with hexane and crystallized from MeOH to afford **8** as a white solid (550 mg, 37%): mp 212 °C; ¹H NMR (CDCl₃): δ 8.95 (s, 2H, H₃), 8.85 (d, 2H, *J* = 8.2 Hz, H₃), 8.68 (d, 2H, *J* = 5.0 Hz, H₆), 8.39 (d, 2H, *J* = 8.7 Hz, H₄), 7.86 (s, 2H, H₅), 7.40 (d, 2H, *J* = 5.5 Hz, H₅), 1.39 (s, 18 H, *t*-Bu);

Ruthenium Catalysts for Water Oxidation Involving Tetradentate Polypyridines

^{13}C NMR (CDCl_3) δ 161.0, 157.1, 156.5, 149.2, 146.0, 137.27, 129.3, 126.9, 121.7, 121.2, 119.1, 35.2, 31.1; MS: $m/z = 447.52$ ($[\mathbf{8}+\text{H}]^+$), 447.60 calcd. for $[\mathbf{8}+\text{H}]^+$.

Complex **4b**(PF_6)₂.

A mixture of **8** (80 mg, 0.18 mmol), $\text{RuCl}_3 \cdot 3\text{H}_2\text{O}$ (47 mg, 0.18 mmol), 4-*t*-butylpyridine (400 mg, 2.96 mmol), triethylamine (0.3 mL) and LiCl (10 mg) was refluxed overnight. After precipitation with NH_4PF_6 (300 mg, 1.83 mmol), the brownish-red residue was chromatographed on alumina eluting with hexane/ CH_2Cl_2 /acetone (1:1:1) followed by recrystallization from $\text{CH}_2\text{Cl}_2/\text{Et}_2\text{O}$ to afford **4b**(PF_6) as a red solid (25 mg, 13%): ^1H NMR (acetone- d_6): δ 10.15 (d, 2H, $J = 5.9$ Hz, H_6), 9.02 (d, 2H, $J = 9.1$ Hz, H_3 or H_4), 8.79 (d, 2H, $J = 8.7$ Hz, H_3 or H_4), 8.71 (s, 2H, H_3), 8.57 (s, 2H, H_5), 8.12 (dd, 2H, $J = 6.8, 1.8$ Hz, H_5), 7.96 (d, 4H, $J = 6.9$ Hz, H_{Pic}), 7.07 (d, 4H, $J = 6.9$ Hz, H_{Pic}), 1.45 (s, 18H, *t*-Bu), 1.00 (s, 18H, *t*-Bu). Anal. calcd. for $\text{C}_{48}\text{H}_{56}\text{F}_{12}\text{N}_6\text{P}_2\text{Ru}$: C, 52.03; H, 5.09; N, 7.58. Found: C, 52.82; H, 4.38; N, 7.37. Complex **4b**(Cl)₂ was prepared by eluting **4b**(PF_6)₂ with methanol through a column containing an ion exchange resin.

2-(Pyrid-2'-yl)-6-(1'',10''-phenanthroline-2''-yl)pyridine (**11**).

A mixture of 6-acetyl-2,2'-bipyridine (**9**, 265 mg, 1.33 mmol) and 8-amino-7-quinolinecarbaldehyde (**10**, 230 mg, 1.34 mmol) was dissolved in EtOH (30 mL) containing KOH (8 mg) and heated at reflux overnight. The reaction mixture was cooled and the residue was purified by chromatography on silica gel, eluting with hexane, CH_2Cl_2 , and $\text{CH}_2\text{Cl}_2/\text{MeOH}$ (2-3%) to provide **11** as an off-white solid (431 mg, 97%), mp 220-221 °C: ^1H NMR (CDCl_3): δ 9.26 (dd, 1H, $J = 4.4, 1.7$ Hz), 9.05 (dd, 1H, $J = 7.8, 1.7$ Hz), 9.04 (d, 1H, $J = 8.2$ Hz), 8.71 (dd,

Ruthenium Catalysts for Water Oxidation Involving Tetradentate Polypyridines

1H, $J = 4.3, 1.7$ Hz), 8.69 (d, 1H, $J = 8.2$ Hz), 8.51 (dd, 1H, $J = 7.8, 1.0$ Hz), 8.41 (d, 1H, $J = 8.2$ Hz), 8.28 (dd, 1H, $J = 8.2, 1.7$ Hz), 8.06 (t, 1H, $J = 7.8, 1.0$ Hz), 7.89 (td, 1H), 7.86 (AB, 2H), 7.69 (dd, 1H, $J = 8.0, 4.4$ Hz), 7.35 (td, 1H, $J = 6.4, 1.0$ Hz); ^{13}C NMR (CDCl_3) δ 156.3, 155.3, 150.5, 149.2, 146.4, 145.8, 138.1, 136.9, 136.3, 129.1, 128.9, 126.9, 126.6, 123.8, 123.0, 122.9, 121.5, 121.3, 121.0.

Complex **6**(Cl)₂

A mixture of **11** (141 mg, 0.42 mmol) and $\text{RuCl}_3 \cdot 3\text{H}_2\text{O}$ (125 mg, 0.48 mmol) in EtOH (40 mL) was heated at reflux for 4 h. Then 4-picoline (0.5 mL), H_2O (10 mL), and Et_3N (0.1 mL) were added and reflux continued overnight. The solvents were evaporated and the residue was chromatographed on alumina, eluting with $\text{CH}_2\text{Cl}_2/\text{MeOH}$ (1:1) with 0-10% added MeOH. The earlier purple fractions were collected and evaporated to yield $[\text{Ru}(\mathbf{11})(\text{pic})_2]\text{Cl}_2$ (150 mg, 52%): ^1H NMR (D_2O): δ 9.83 (d, 1H, $J = 4.6$ Hz), 9.70 (d, 1H, $J = 5.4$ Hz), 8.61 (d, 1H, $J = 9.2$ Hz), 8.53 (d, 1H, $J = 8.2$ Hz), 8.41 (d, 1H, $J = 7.2$ Hz), 8.37 (d, 1H, $J = 9.2$ Hz), 8.18 (d, 1H, $J = 8.2$ Hz), 8.07 (d, 1H, $J = 8.2$ Hz), 7.96–7.85 (m, 5H), 7.78 (dd, 1H, $J = 5.4, 6.4$ Hz), 7.63 (d, 4H, $J = 6.4$ Hz), 6.58 (d, 4H, $J = 6.4$ Hz), 1.85 (s, 6H). Anal. calcd. for $\text{C}_{34}\text{H}_{28}\text{N}_6\text{Cl}_2\text{Ru} \cdot 3\text{H}_2\text{O}$: C, 54.69; H, 4.59; N, 11.26. Found: C, 54.81; H, 4.81; N, 11.37. MS (ESI): $m/z = 311.07$ ($[\mathbf{6}]^{2+}$), 311.07 calcd. for $[\mathbf{6}]^{2+}$.

Complex **6**(ClO₄)₂

A few drops of aqueous NaClO_4 (sat.) was added to a water solution (4 mL) of **6**(Cl)₂ (29 mg). The mixture was stirred at room temperature for 1 h. The precipitate was collected and dried in an oven to yield **6**(ClO₄)₂ (27 mg, 80%).

Acknowledgment. This work was funded by the Division of Chemical Sciences, Geosciences, and Biosciences, Office of Basic Energy Sciences of the U.S. Department of Energy through Grant DE-FG02-07ER15888. We also thank the Robert A. Welch Foundation (E-621) for support.

Supporting Information. ¹H NMR spectra for **4b** and **6**, UV-vis spectra, crystal data, electrochemical waves, O₂ evolution plots for kinetic analyses and mass spectra.

References

- (1) (a) Concepcion, J. J.; Tsai, M. -K.; Muckerman, J. T.; Meyer, T. J. *J. Am. Chem. Soc.* **2010**, *132*, 1545–1557. (b) Blakemore, J. D.; Schley, J. D.; Balcells, D. Hull, J. F.; Olack, G. W.; Incarvito, C. D.; Eisenstein, O.; Brudvig, G. W.; Crabtree, R. H. *J. Am. Chem. Soc.*, **2010**, *132*, 16017–16029. (c) Leung, C.-F.; Ng, S.-M.; Ko, C.-C.; Man, W.-L.; Wu, J.; Chen, L.; Lau, T.-C. *Energy Environ. Sci.* **2012**, *5*, 7903–7907. (d) Hetterscheid, D. G. H.; Reek, J. N. H. *Angew. Chem. Int. Ed.* **2012**, *51*, 9740-9747. (e) Radaram, B.; Ivie, J. A.; Singh, W. M.; Grudzien, R. M.; Reibenspies, J. H.; Webster, C. E.; Zhao, X. *Inorg. Chem.* **2011**, *50*, 10564-10571. (f) Roeser, S.; Farras, P.; Bozoglian, F.; Martinez-Belmonte, M.; Benet-Buchholz, J.; Llobet, A. *ChemSusChem* **2011**, *4*, 197-207. (g) Savini, A.; Ballachioma, G.; Ciancaleoni, G.; Zuccaccia, C.; Zuccaccia, D.; Macchioni, A. *Chem. Commun.* **2010**, *46*, 9218-9219. (h) Concepcion, J. J.; Jurss, J. W.; Norris, M. R.; Chen, Z.; Templeton, J. L.; Meyer, T. J. *Inorg. Chem.* **2010**, *49*, 1277-1279. (i) Concepcion, J. J.; Jurss, J. W.; Templeton, J. L.; Meyer, T. J. *J. Am. Chem. Soc.* **2008**, *130*, 16462-16463. (j) Cao, R.; Lai, W.; Du, P. *Energy Environ. Sci.* **2012**, *5*, 8134-8157.

Ruthenium Catalysts for Water Oxidation Involving Tetradentate Polypyridines

- (2) Zong, R.; Thummel, R. P. *J. Am. Chem. Soc.* **2005**, *127*, 12802–12803.
- (3) (a) Tseng, H.-W.; Zong, R.; Muckerman, J. T.; Thummel, R. *Inorg. Chem.* **2008**, *47*, 11763–11773. (b) Yagi, M.; Tajima, S.; Komi, M.; Yamazaki, H. *Dalton Trans.* **2011**, 3802–3804. (c) Wasylenko, D. J.; Ganesamoorthy, C.; Henderson, M. A.; Berlinguette, C. P. *Inorg. Chem.* **2011**, *50*, 3662–3672. (d) Masaoka, S.; Sakai, K. *Chem. Lett.* **2009**, *38*, 182–183. (e) Wasylenko, D. J.; Ganesamoorthy, C.; Kovisto, B. D.; Henderson, M. A.; Berlinguette, C. P. *Inorg. Chem.* **2010**, *49*, 2202–2209. (f) Wasylenko, D. J.; Ganesamoorthy, C.; Henderson, M. A.; Koivisto, B. D.; Osthoff, H. D.; Berlinguette, C. P. *J. Am. Chem. Soc.* **2010**, *132*, 16094–16106.
- (4) Kaveevivitchai, N.; Zong, R.; Tseng, H.-W.; Chitta, R.; Thummel, R. P. *Inorg. Chem.* **2012**, *51*, 2930–2939.
- (5) (a) Zong, R.; Thummel, R. P. *J. Am. Chem. Soc.* **2004**, *126*, 10800–10801. (b) Zhang, G.; Zong, R.; Tseng, H.-W.; Thummel, R. P. *Inorg. Chem.* **2008**, *47*, 990–998.
- (6) Deng, Z.; Tseng, H.W.; Zong, R.; Wang, D.; Thummel, R. *Inorg. Chem.* **2008**, *47*, 1835–1848.
- (7) (a) Duan, L.; Fischer, A.; Xu, Y.; Sun, L. *J. Am. Chem. Soc.* **2009**, *131*, 10397–10399. (b) Tong, L.; Duan, L.; Xu, Y.; Privalov, T.; Sun, L. *Angew. Chem., Int. Ed.* **2011**, *50*, 445–449. (c) Duan, L.; Bozoglian, F.; Mandal, S.; Stewart, B.; Privalov, T.; Llobet, A. *Nat. Chem.*, **2012**, *4*, 418–423.
- (8) Muckerman, J. T.; Kowalczyk, M.; Badiei, Y. M.; Polyansky, D. E.; Concepcion, J. J.; Zong, R.; Thummel, R. P.; Fujita, E. *Inorg. Chem.* **2014**, *53*, 6904–6913.
- (9) Duan, L.; Xu, Y.; Tong, L.; Sun, L. *ChemSusChem* **2011**, *4*, 238–244.
- (10) Concepcion, J. J.; Tsai, M.; Muckerman, J. T.; Meyer, T. J., *J. Am. Chem. Soc.* **2010**, *132*, 1545–1557.
- (11) Zong, R.; Wang, B.; Thummel, R. P. *Inorg. Chem.* **2012**, *51*, 3179–3185.
- (12) (a) Given, K. W.; Mattson, B. M.; Pignolet, L. H. *Inorg. Chem.* **1976**, *15*, 3152–3156. (b) Mattson, B. M.; Pignolet, L. H. *Inorg. Chem.* **1977**, *16*, 488–491.

Ruthenium Catalysts for Water Oxidation Involving Tetradentate Polypyridines

(13) (a) Masllorens, E.; Rodriguez, M.; Romero, I.; Roglans, A.; Parella, T.; Benet-Buchholz, J.; Poyatos, M.; Llobet, A. *J. Am. Chem. Soc.* **2006**, *128*, 5306–5307. (b) Huynh, M. H. V.; Meyer, T. J. *Chem. Rev.* **2007**, *107*, 5004–5064.

(14) (a) Kaveevivitchai, N.; Chita, R.; Zong, R.; Ojami, M. E.; Thummel, R. P. *J. Am. Chem. Soc.* **2012**, *134*, 10721–10724. (b) Li, F.; Yi, J.; Zhang, B.; Huang, F.; Gao, Y.; Sun, L. *Angew. Chem., Int. Ed.* **2012**, *51*, 2417–2420. (c) Ashford, D. L.; Stewart, D. J.; Glasson, C. R.; Binstead, R. A.; Harrison, D. P.; Norris, M. R.; Concepcion, J. J.; Fang, Z.; Templeton, J. L.; Meyer, T. J. *Inorg. Chem.* **2012**, *51*, 6428–6430. (d) Hara, M.; Waraksa, C. C.; Lean, J. T.; Lewis, B. A.; Mallouk, T. E., *J. Phys. Chem. A* **2000**, *104*, 5275–5280.

(15) White, H. S.; Becker, W. G.; Bard, A. J. *J. Phys. Chem.* **1984**, *88*, 1840–1846.

(16) Crabtree, R. H. *Chem. Rev.* **2012**, *112*, 1536–1554.

(17) (a) Duan, L.; Xu, Y.; Zhang, P.; Wang, M.; Sun, L. *Inorg. Chem.* **2010**, *49*, 209–215. (b) Duan, L.; Xu, Y.; Zhang, P.; Wang, M.; Sun, L. *Inorg. Chem.* **2010**, *49*, 209–215. (c) Xu, Y.; Duan, L.; Tong, L.; Åkermark, B.; Sun, L. *Chem. Commun.* **2010**, *46*, 6506–6508.

(18) Ghosh, P. K.; Brunschwig, B. S.; Chou, M.; Creutz, C.; Sutin, N. *J. Am. Chem. Soc.* **1984**, *106*, 4772–4783.

(19) Yamada, M.; Nakamura, Y.; Kuroda, S.; Shima, I. *Bull. Chem. Soc. Jpn.* **1990**, *63*, 2710–2712.

(20) Constable E. C.; Heirtzler F.; Neuburger M.; Zehnder M. *J. Am. Chem. Soc.* **1996**, *119*, 5606–5617.

(21) Riesgo, E. C.; Jin, X.; Thummel, R. P. *J. Org. Chem.*, **1996**, *61*, 3017–3022.